Theoretical Investigation of the Nature of Aluminum-Containing Species Present in Alkaline Solution

Julian D. Gale,*,† Andrew L. Rohl,‡ Helen R. Watling,§ and Gordon M. Parkinson‡

Department of Chemistry, Imperial College of Science, Technology and Medicine, South Kensington, SW7 2AY, U.K., A. J. Parker Cooperative Research Centre for Hydrometallurgy, School of Applied Chemistry, Curtin University of Technology, P.O. Box U1987, Perth, Western Australia 6845, and A. J. Parker Cooperative Research Centre for Hydrometallurgy, CSIRO Minerals, P.O. Box 90, Bentley, Western Australia 6982

Received: July 16, 1998

The structure, energies, and infrared spectra of a range of possible monomeric and dimeric aluminum-containing neutral and anionic species that may be present in either dilute or concentrated alkaline sodium aluminate solutions have been studied using ab initio methods at the MP2/6-31G**, B3LYP/6-31G**, and B3LYP/6-311++G**//B3LYP/6-31G** levels. Results are presented for the species in vacuo and with a representation of the surrounding environment using either a self-consistent polarizable continuum model or a charge-compensating electrostatic potential of varying magnitude to represent high levels of ion concentration. Both predicted energetics and infrared spectra confirm that the dominant species present under dilute aqueous conditions is the $Al(OH)_4(H_2O)_4^-$ anion. At high concentrations of sodium aluminate, it is predicted that dimerization to the doubly hydroxyl-bridged species $(OH)_3Al(OH)_2Al(OH)_3^{2-}$ can occur and that this is assisted by the coordination of two or more water molecules.

1. Introduction

The industrially important Bayer process leads to the production of alumina from bauxite via high-temperature digestion in concentrated caustic soda followed by precipitation of the gibbsite polymorph of $Al(OH)_3$ and subsequent calcination. Although this process is over 100 years old, the underlying fundamental chemistry is poorly understood. Hypotheses about the aluminate ion species distribution in concentrated caustic aluminate solutions abound in the literature, indicating the importance attached to this topic by those concerned with this process.[1,2] The importance lies in their relevance to the unusually slow precipitation stage, as this is the single most rate-limiting step in the Bayer process, leading to large capital and operating costs. Although improvements in gibbsite precipitation have been achieved over the years by incremental process modifications, a fundamental understanding of the species distribution in aluminate solutions, particularly those species which hinder or promote the crystal growth process, is essential if further significant advances in productivity are to be made.

The focus of many spectroscopic studies has been the identification and sometimes quantification of aluminate ions in pure solutions at industrially relevant concentrations. The use of infrared, Raman, ^{27}Al solution NMR, and UV−visible spectroscopies has been reported. However, interpretations founded on UV−visible spectrophotometric data can be discounted because aluminate ions in pure solutions have no UV signal.[3]

It is generally agreed that, in dilute alkaline aluminate solutions, the aluminate ion is $Al(OH)_4^-$ with four-fold aluminum coordination.[4,5] Concerning more concentrated alkaline aluminate solutions there is some discord, but the vast majority of researchers concur with Moolenaar et al.[5] that a second aluminate ion species, the oxo-bridged dimer, $[(OH)_3AlOAl(OH)_3]^{2-}$, exists in equilibrium with $Al(OH)_4^-$. In one case a "dimerization" constant has been calculated on the assumption that only these two aluminate-ions exist in solution.[6]

The conclusion of Moolenaar et al.[5] is based on the strong similarity between the spectra of concentrated aluminate solutions and of crystalline potassium aluminate, which contains the dimeric aluminate grouping in its crystal.[7] However, a simple, two-anion theory alone cannot describe the mechanism by which gibbsite, with its layered, hexagonal structure in which the aluminum atoms have six-fold coordination geometry and are linked by double hydroxo bridges,[8] precipitates spontaneously from pure, unseeded caustic aluminate solutions supersaturated in respect of aluminum.[9] Similarly, in growth onto gibbsite seeds which occurs during the Bayer process, it is likely that at least intermediate structures occur during the incorporation of the dominant $Al(OH)_4^-$ solution species into the gibbsite lattice.

In addition to $Al(OH)_4^-$ and $[(OH)_3AlOAl(OH)_3]^{2-}$, anions such as $Al(OH)_6^{3-}$, the hexameric $Al_6(OH)_{24}^{6-}$ ion, "polymers", "clusters", and sodium−aluminate ion pairs have been proposed from ^{27}Al solution NMR data[10−13] and from fits to conductivity and viscosity data,[14] broadening the possible speciation to the point where a mechanism which accounts for some of the necessary steps in gibbsite precipitation; for example, the transformation from four- to six-fold aluminum coordination geometry and the formation of hydroxo bridges between aluminum atoms could be proposed. However, the spectra on which these interpretations are based often exhibit features such

* Author to whom correspondence should be addressed.
† Imperial College of Science, Technology and Medicine.
‡ A. J. Parker Cooperative Research Centre for Hydrometallurgy, School of Applied Chemistry.
§ A. J. Parker Cooperative Research Centre for Hydrometallurgy, CSIRO Minerals.

10.1021/jp983044r CCC: $15.00
Published on Web 11/14/1998

as extreme line broadening and missing signal intensities. Even where a systematic study has been made, the data are equivocal and, generally, hypotheses are not supported by independent evidence.

In this work, the relative stability of most of the possible monomeric and dimeric aluminate anions is examined using ab initio quantum mechanics with the aim of describing the species present in caustic aluminate solutions. Previous work in this area has been restricted to the use of semi-empirical methods,[15] whose accuracy is uncertain, or to the application of higher-level techniques to only a small subset of the possible anions.[16−18] Here, calculations have been performed for the gas phase and with corrections to describe both the dilute solution and concentrated liquor limits, as the effect of the environment cannot be ignored when considering such species. Finally, the calculated infrared spectra are compared with the experimental observations to see if the stability predictions can be reconciled with the spectroscopic evidence.

2. Methods

This study is focused on the nature of the aluminum-containing species that exist in alkaline solutions. Hence, it is restricted to species which are either neutral or negatively charged, as it is highly unlikely that any cationic forms of aluminum will be present. There are already a large number of studies of the $Al(OH)_4^-$ aluminate ion and its protonated form, especially in the context of modeling Brønsted acid sites in zeolites.[16−20] However, far less work has been performed on the other possible aluminum-containing anions that may exist under basic conditions. Hence, ab initio quantum mechanical results for a range of monomeric and dimeric species with aluminum coordination numbers varying from two to six are presented here.

Although preliminary geometry optimizations were performed at the Hartree−Fock level, the final results presented include corrections for electron correlation through either second-order Møller−Plesset theory (MP2) or Becke's three-parameter combination of Hartree−Fock and gradient-corrected density functional exchange combined with the nonlocal correlation functional of Lee−Yang−Parr (B3LYP).[21,22] In the case of the MP2 results, only valence orbitals are included in the active space. Previous works have demonstrated that for most ground state properties of a wide range of compounds, the gradient-corrected density functional formalism gives results of quality comparable to those of an MP2 calculation.[23] If this can be validated for the species of interest here, then the scope of the calculations for tackling larger polymeric species will be increased due to the lower computational demands of the B3LYP approximation. Although a pure gradient-corrected density functional, with no calculation of the Hartree−Fock exchange, would be even more economical, the B3LYP functional has been shown to be generally more reliable.[24]

The majority of calculations have been performed using the standard double-ζ 6-31G** basis set which includes polarization functions for all elements.[25] Although larger basis sets are desirable, there is often found to be some cancellation of errors between the incompleteness of the correlation correction and that of the basis set. For instance, Kubicki et al.[5] found that MP2/6-31G* calculations reproduced the proton affinity of the $Al(OH)_4^-$ anion as calculated with the far more extensive G2 method to within 15 kJ mol^{-1}. As many of the species involved are anions, the addition of diffuse functions will be important, particularly for oxygen, in order to obtain accurate energetics. However, the influence of basis set on geometry is found to be smaller. Hence, in order to make the full optimization and frequency evaluation possible for all species at the same level of accuracy, these tasks have been undertaken at the double-ζ polarization level, with a more extensive basis set being used for a single-point energy evaluation at the final configuration (B3LYP/6-311++G**//B3LYP/6-31G**). All calculations were performed using the program Gaussian94.[26]

The optimization of all clusters was started, initially, from the most symmetric geometry possible in order to minimize computational expense. Subsequently, the vibrational frequencies were calculated, and if any imaginary eigenvalues were found to be present the geometry was perturbed along the appropriate eigenvector(s) and reminimized. This procedure was continued until the Hessian matrix was positive definite and a genuine minimum had been located. Given that some of the species have relatively soft modes, it was necessary to use the analytical Hessian in many cases to achieve highly converged optimizations.

Vibrational frequencies were calculated for all species at the MP2(fc)/6-31G** and B3LYP/6-31G** levels, and the resulting zero-point energies have been used to correct all reported reaction energies. In the case of energy differences calculated at the B3LYP/6-311++G**//B3LYP/6-31G** level, the difference in zero-point energies at the B3LYP/6-31G** level has been used as an approximate correction.

Where possible, analytical second derivatives have been used to calculate the vibrational frequencies. However, for a few of the largest dimer species at the MP2 level it was necessary to use numerical frequencies, calculated by central finite differencing of the analytical forces, as the amount of disk space required exceeded the amount available even in the most disk-efficient algorithm.

An important aspect of this work is the environment in which the aluminum species exist. Many of the anions are likely to be unstable in the gas phase (particularly those with multiple negative charges) but may possibly be formed in solution. Experimentally, aluminate solutions have been studied both in the case of dilute solutions and for concentrated liquors where the number of water molecules may only be of the order of four per cation or anion. Clearly, two such diverse situations will require different approaches to their simulation.

2.1. Dilute Solutions. There are a number of possible approaches to modeling dilute solutions. One is the use of a combined QM/MM strategy in which the quantum mechanically treated aluminum species is immersed in a supercell of water whose interactions are included using classical interatomic potentials. A range of configurations of surrounding water molecules can then be sampled using either Monte Carlo or molecular dynamics techniques. Such an approach provides a high level of insight into the solvation of the species. However, it would be prohibitively expensive to perform for a large number of different molecules and anions, as is the case in this study. Furthermore, unless the full range of solvent configurations were sampled, the energy differences might be artificially biased by the initial configuration assigned to the solvent molecules.

A more economical strategy, which has been widely applied for organic and inorganic systems,[27,28] is to embed the species in a dielectric continuum which possesses the dielectric constant of water. Several different formalisms exist within this general category of methodologies with varying levels of sophistication, particularly with respect to the location of the boundary between the molecule and the solvent. For the purposes of this study, the dilute solution limit has been treated by the SCI-PCM

approach,[29] in which the polarization of the solvent is included self-consistently. Although it is desirable to optimize the species in the presence of the dielectric, the solvation energy has been calculated as a single-point correction at the gas-phase minimum energy configuration because of computational restrictions.

As specific hydrogen bonds may form between the aluminate species and water, it is preferable to treat the first solvation shell explicitly and then embed the total system in the dielectric medium, as has been demonstrated for a number of systems.[30] At the present time, this is not practical for all the species under consideration. However, in some cases the consequences of including specific water molecules have been investigated.

2.2. Concentrated Solutions. At the other extreme, the concentrated Bayer liquor (a typical composition would be 4 M NaOH and 2.5 M Al) cannot be regarded as a dilute solution, as there are insufficient water molecules to satisfy the hydration needs of the ions in solution. Embedding in a dielectric continuum would be inappropriate in this regime as the dominant interaction is the Coulomb potential acting between cations and anions, rather than solvation. Furthermore, the dielectric constant for such a medium would be very different from water, and it is experimentally unknown. Because of the high concentration of charged species it is more reasonable to regard the sodium aluminate liquors as an amorphous "lattice". Critically, it is necessary to incorporate the influence of the electrostatic potential of the counter-cations when determining the relative stabilities of different anions.

As a first approximation, each ion on average would be expected to experience the influence of an equal charge, but of opposite sign, due to the surrounding counterions, to maintain electroneutrality. The distance to which two ions of opposite charge can approach would depend on the extent of hydration and, in particular, the number of shells of solvent molecules around each species. Based on this, the following model is proposed as an approximate method for examining the relationship between the stability of an anion and the number of hydration shells of water (which is in turn related to the amount water actually available in such highly concentrated solutions). The presence of the countercations around each anion is represented by a series of point-charges distributed over the surface of a sphere, centred on the centre of mass, with equal partial charges such that the total charge balances that of the anion. This construction ensures that there are no low order multipole moments which might give rise to preferred relative orientations between the point-charges and the enclosed anion.

The radius of the point-charge sphere is determined as follows. First, the maximum diameter of the anion is calculated on the basis of Van der Waals radii for the constituent atoms, and this is divided by two to obtain an effective radius for the species. A number of alternative approaches for obtaining a radius were examined on the basis of properties of the underlying quantum mechanical calculations. However, this simple approach appears to give the most consistent pattern of radii between different species. The same approach has been used to determine the diameter of a water molecule, while the ionic radius was used for a sodium cation. From the appropriate sum of the radii, the radius of the point-charge sphere can be calculated for any given number of hydration shells. For example, if two solvent shells separate the cation−anion pair then the radius is set equal to the sum of the sodium and anion radii, plus twice the diameter of a water molecule.

To examine the effect of the degree of hydration, this Coulomb stabilization has been calculated for the cases where there is no water of solvation or one, two, and three shells of water. These four cases correspond to radii of 1.16, 5.07, 8.98, and 12.89 Å, respectively, plus the radius of the species itself. Clearly, in the case of no water of solvation, the results are at their most approximate, as strictly speaking in such a situation explicit inclusion of sodium is necessary. However, based on calculations where sodium cations have been included, which will be presented in a subsequent publication, the results for the no water of solvation case turn out to be qualitatively correct. Given, that it is hard to specify an unambiguous radius for each solvent shell, the results to be presented are best considered as points sampled along a continuous function, though the direct correlation of radius to water concentration is hard to calibrate.

Although it is straightforward to calculate the energy of interaction between each anion and the four sets of point-charge arrays considered in this study through an explicit quantum mechanical calculation, it turns out that this term can be evaluated more economically and with negligible loss of accuracy. This is achieved by using electrostatic potential fitted point-charges to represent the anion[31], subject to the constraint that the dipole moment of the molecule is correctly reproduced, in a direct sum over the Coulomb interactions. The ESP charges were determined from the B3LYP/6-31G** electron density.

The interaction between the partially charged point ions is excluded when calculating the electrostatic energy. However, in the case of multiply charged anions there would also be a term for the repulsion between cations. To correct for this, the electrostatic energy that would exist between sodium cations is added on, assuming they were situated on the surface of the sphere so as to maximize the distance between them.

3. Results and Discussion

The total energies for all optimized species, including monomers and dimers, and their zero-point energies are tabulated for the gas phase in Table 1 for both the MP2(fc) and B3LYP methods using a 6-31G** basis set. Also included in Table 1 are the single-point energies determined at the B3LYP/6-311++G** level. In addition, the energies of all species when embedded in a dielectric continuum are given in Table 2, while the energies when surrounded by the charge compensating electrostatic field are listed in Table 3.

3.1. Monomer Species. The geometries for the monomer species calculated by the hybrid density functional approach are illustrated in Figure 1, with key bond lengths and bond angles being indicated. In the case of the species $AlO(OH)_2^-$, there are three possible conformations that may exist in which the hydroxyl groups are in different permutations of cis and trans orientations relative to the Al═O group. The geometries of the two extremes of both cis or both trans have been calculated for comparison. Other species may also have more than one configuration of hydroxyl orientations, though the differences are more subtle than for $AlO(OH)_2^-$. Hence, in general, the most stable arrangement located has been considered.

The geometries of the monomeric clusters show the trends that would be expected and that were observed in a previous study of the aluminate anion together with neutral and positively charged species.[18] The Al−O bond length is at a minimum for AlO_2^- with a value of 1.638 Å, closely followed by the Al−O double bond in $AlO(OH)_2^-$, while the longest bonds are close to 2.01 Å in $Al(OH)_5^{2-}$ and $Al(OH)_6^{3-}$. This demonstrates the increasing bond length as the coordination number rises. In gibbsite itself, the Al−O bond length has a mean value of 1.90 Å[32] which is lower than for the octahedral monomer, which is to be expected as it lacks the large overall negative charge which

TABLE 1: Total Energies (au) and Zero-Point Energies (au) for All Species at the MP2(fc)/6-31G, B3LYP/6-31G**, and B3LYP/6-311++G**//B3LYP/6-31G** Levels of Calculation; the Zero-Point Energies Are the Unscaled Values**

	MP2(fc)/6-31G**		B3LYP/6-31G**		B3LYP/6-311++G**
cluster	total energy	ZPE	total energy	ZPE	total energy
H_2O	−76.219786	0.021878	−76.419737	0.021358	−76.458476
OH^-	−75.526070	0.008417	−75.726292	0.007965	−75.827198
AlO_2^-	−392.088186	0.005484	−392.933120	0.005589	−393.040277
$AlO(OH)_2^-$ cis	−468.414836	0.030588	−469.461331	0.030186	−469.594443
$AlO(OH)_2^-$ trans	−468.406151	0.029760	−469.452602	0.029283	−469.585718
$Al(OH)_3$	−469.025998	0.041725	−470.071651	0.041119	−470.185653
$Al(OH)_3(H_2O)$	−545.290418	0.068149	−546.534337	0.066926	−546.675099
$Al(OH)_4^-$	−544.750246	0.054803	−545.994802	0.053936	−546.154865
$Al(OH)_4(H_2O)^-$	−621.005110	0.081638	−622.449710	0.080240	−622.640003
$Al(OH)_4(H_2O)_2^-$	−697.255049	0.107866	−698.899398	0.105995	−699.123842
$Al(OH)_4(H_2O)_4^-$	−849.746222	0.161549	−851.794422	0.158964	−852.077443
$Al(OH)_5^{2-}$	−620.223735	0.070206	−621.667320	0.068966	−621.887396
$Al(OH)_5(H_2O)^{2-}$	−696.502947	0.097061	−698.145933	0.095029	−698.394253
$Al(OH)_6^{3-}$	−695.529103	0.084350	−697.173004	0.083132	−697.470577
$Al_2(OH)_6$	−938.163243	0.087364	−940.246003	0.086225	−940.456089
$Al_2(OH)_7^-$	−1013.878719	0.100924	−1016.163525	0.099423	−1016.419017
$Al_2(OH)_8^{2-}$	−1089.427603	0.115425	−1091.906904	0.113450	−1092.218243
$Al_2(OH)_8(H_2O)_2^{2-}$	−1241.958885	0.170822	−1244.837512	0.168111	−1245.206690
$Al_2O(OH)_6^{2-}$	−1013.181170	0.089255	−1015.465164	0.087862	−1015.739371
$Al_2O_2(OH)_4^{2-}$	−936.892616	0.063869	−938.974928	0.062899	−939.218081

TABLE 2: Hydration Energies (kJ mol^{-1}) for All Species at the B3LYP/6-31G and B3LYP/6-311++G** Levels of Calculation, Determined at the Optimized B3LYP/6-31G** Gas-Phase Geometry Using the SCI-PCM Model with a Dielectric Constant of 80.4 for Water**

cluster	B3LYP/6-31G**	B3LYP/6-311++G**
H_2O	−22.032	−21.473
OH^-	−341.282	−274.724
AlO_2^-	−237.229	−221.918
$AlO(OH)_2^-$ cis	−236.542	−222.275
$AlO(OH)_2^-$ trans	−251.530	−235.393
$Al(OH)_3$	−34.970	−37.052
$Al(OH)_3(H_2O)$	−47.233	−45.753
$Al(OH)_4^-$	−222.804	−203.338
$Al(OH)_4(H_2O)^-$	−209.434	−195.146
$Al(OH)_4(H_2O)_2$	−200.493	−181.638
$Al(OH)_4(H_2O)_4^-$	−196.695	−177.855
$Al(OH)_5^{2-}$	−800.984	−734.561
$Al(OH)_5(H_2O)^{2-}$	−741.822	−679.760
$Al(OH)_6^{3-}$	−1716.043	−1558.915
$Al_2(OH)_6$	−59.609	−59.630
$Al_2(OH)_7^-$	−209.492	−191.739
$Al_2(OH)_8^{2-}$	−672.487	−616.678
$Al_2(OH)_8(H_2O)_2^{2-}$	−628.454	−579.213
$Al_2O(OH)_6^{2-}$	−694.410	−639.900
$Al_2O_2(OH)_4^{2-}$	−720.382	−685.097

TABLE 3: Electrostatic Stabilization Energies (kJ mol^{-1}), for Cation Distributions at Radii Consistent with Different Numbers of Solvation Shells, for All Species at the B3LYP/6-31G Level of Calculation[a]**

cluster	0 shells	1 shell	2 shells	3 shells
OH^-	−457.633	−199.776	−127.850	−94.013
AlO_2^-	−330.256	−171.324	−115.601	−87.226
$AlO(OH)_2^-$ cis	−306.193	−164.520	−112.453	−85.419
$AlO(OH)_2^-$ trans	−282.034	−157.354	−109.027	−83.413
$Al(OH)_4^-$	−301.592	−163.241	−111.862	−85.080
$Al(OH)_4(H_2O)^-$	−264.961	−151.739	−106.334	−81.844
$Al(OH)_4(H_2O)_2^-$	−231.484	−140.031	−100.473	−78.332
$Al(OH)_4(H_2O)_4^-$	−230.614	−139.379	−100.149	−78.138
$Al(OH)_5^{2-}$	−1051.227	−569.872	−390.805	−297.362
$Al(OH)_5(H_2O)^{2-}$	−886.803	−517.533	−365.449	−282.449
$Al(OH)_6^{3-}$	−2215.046	−1191.251	−815.151	−619.577
$Al_2(OH)_7^-$	−232.600	−140.503	−100.687	−78.456
$Al_2(OH)_8^{2-}$	−824.262	−495.185	−354.135	−275.639
$Al_2(OH)_8(H_2O)_2^{2-}$	−816.829	−493.077	−353.096	−275.017
$Al_2O(OH)_6^{2-}$	−846.288	−503.986	−358.654	−278.376
$Al_2O_2(OH)_4^{2-}$	−916.200	−527.895	−370.611	−285.528

[a] All species with zero charge are excluded from the table as the energy is always zero.

causes extra repulsion between oxygens. For most of the species the O−H bond length lies between 0.960 and 0.965 Å. However, for the two multiply charged anions the values are significantly longer by 0.01 Å.

For the species $Al(OH)_4^-$ and $Al(OH)_3(H_2O)$, the optimized geometries determined in this work are generally close to those published by Kubicki et al.[17] at the MP2/6-31G* level, though typically the bond lengths are just a little smaller here due to the extra polarization functions on hydrogen. Although often referred to as being tetrahedral, the $Al(OH)_4^-$ is actually flattened along one axis and adopts the point group S_4. However, dynamical effects will lead to apparent tetrahedral behavior. Thus, when water or sodium is coordinated to the aluminate anion, a significant perturbation of the geometry occurs, leading to weakening of the bonds from aluminum to the oxygen atoms which are involved in the interaction.

3.1.1. Stability of Monomers in the Gas Phase and Dilute Solution. A number of possible solution equilibria can be conceived for monomeric species, corresponding to the loss or gain of water or hydroxyl groups. These reactions are illustrated in Scheme 1. Reactions 1−3 represent the addition of hydroxyl anions to form increasingly charged anions up to the limit where aluminum is octahedrally coordinated by OH^-. Reactions 4−7 are concerned with the possibility of dehydration of $Al(OH)_4^-$ to form lower coordinated alumina species in which Al−O double bonds are nominally formed. In reactions 8−11, the possibility that aluminum may bind extra water molecules to achieve up to six-fold coordination is considered. Finally, in reaction 12, four water molecules are added so that each hydrogen bonds to one hydroxyl oxygen, thus including the first hydration shell explicitly. It is important to note that water will bind to the oxygen of the hydroxyl groups in preference to hydrogen bonding via oxygen of water to a hydrogen of the alumina species. This is in accord with results obtained for the hydration of OH^- where the ion shows little tendency to form hydrogen bonds through the hydrogen.[33]

Reaction energies for all 12 processes are given in Table 4 for the cases where they occur in the gas phase and in dilute solution using the self-consistent polarizable continuum model. Comparison of the MP2(fc) and B3LYP reaction energies, for

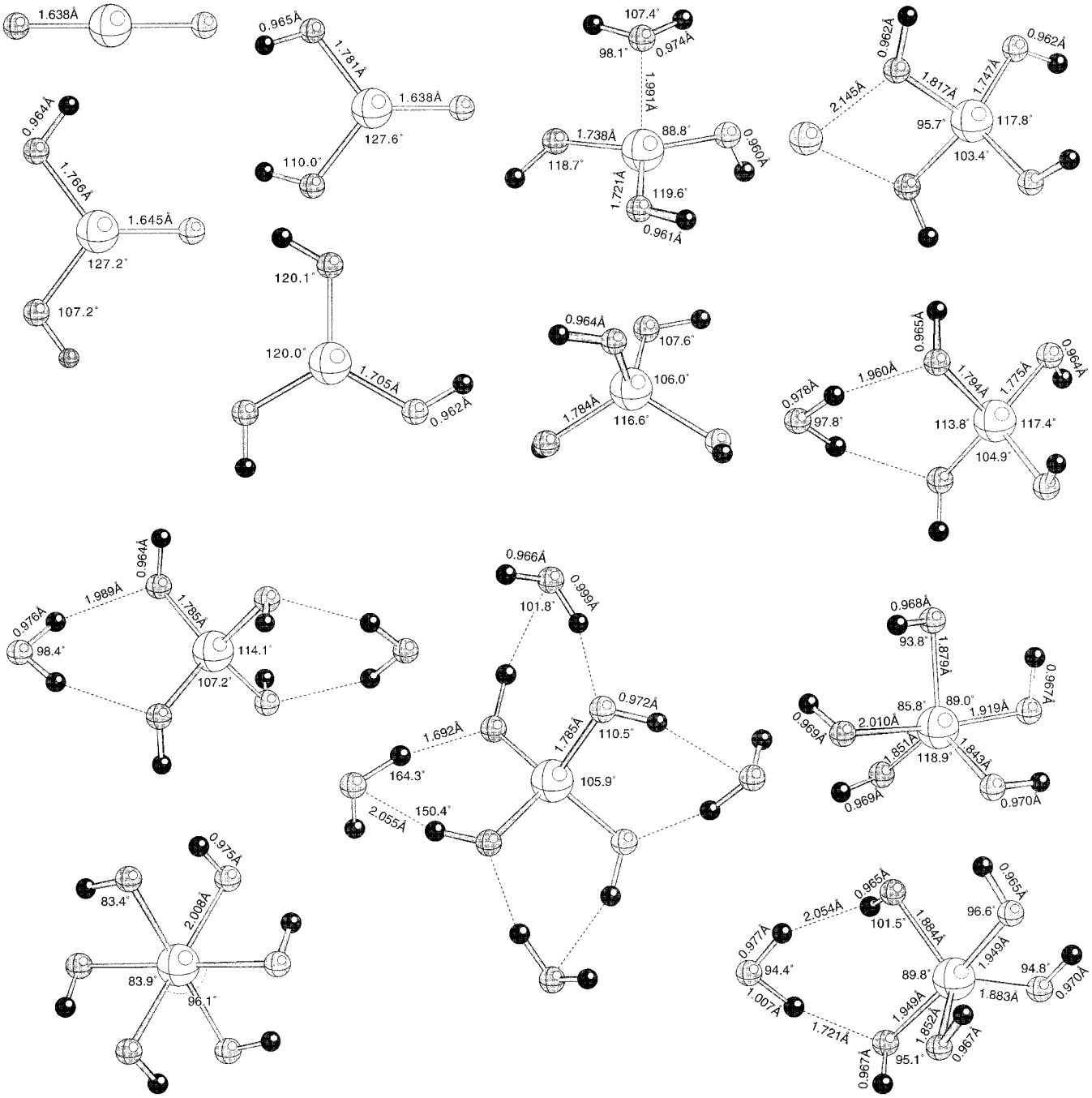

Figure 1. Optimized structures at the B3LYP/6-31G** level of calculation for the monomeric aluminate species, including selected symmetry unique bond lengths and angles. Aluminum atoms are colored in light grey, oxygen in mid-grey, and hydrogens are dark grey.

the same basis set, shows that they are generally very close and always agree to within the 2 kcal target accuracy which is a realistic aim for quantum mechanical methods. However, the importance of extensive basis sets when treating anions is clearly demonstrated in the energy differences between values calculated at the B3LYP/6-31G** and B3LYP/6-311++G** levels. Based on this, the discussion of reaction energies in solution will be restricted to the B3LYP/6-311++G** values. It is also worth noting that the density functional calculations were far more readily convergent when combined with the self-consistent polarization field than were the MP2(fc) equivalents.

Examination of the results for the equilibria involving successive hydroxyl additions to $Al(OH)_3$ show that, in the gas phase, the formation of $Al(OH)_4^-$ would be strongly favored due to the distribution of the excess negative charge over more electronegative atoms. Formation of multiply charged anions is clearly impossible in the gas phase as the electrostatic repulsion dominates all other interactions.

Consider the situation in dilute solution as represented by the use of a dielectric continuum model. As would be expected, the combination of $Al(OH)_3$ and OH^- is now significantly less exothermic than in the gas phase as the solvation energy is maximized by small highly charge ions. The most significant change is that the addition of a second hydroxyl group to the tetrahedral aluminate ion, to form a five-coordinate species, is now found to be only moderately endothermic. While this is consistent with the experimental observation that the most abundant aluminum species in dilute basic solutions is the $Al(OH)_4^-$ ion, it also suggests that a small concentration of $Al(OH)_5^{2-}$ may be possible. With only the double-ζ plus

SCHEME 1: Reaction Scheme for Possible Equilibria between Monomeric Alumina Species in Alkaline Solution

(1) $Al(OH)_3 + OH^- \Leftrightarrow Al(OH)_4^-$

(2) $Al(OH)_4^- + OH^- \Leftrightarrow Al(OH)_5^{2-}$

(3) $Al(OH)_5^{2-} + OH^- \Leftrightarrow Al(OH)_6^{3-}$

(4) $AlO_2^- + H_2O \Leftrightarrow cis\text{-}AlO(OH)_2^-$

(5) $AlO_2^- + H_2O \Leftrightarrow trans\text{-}AlO(OH)_2^-$

(6) $cis\text{-}AlO(OH)_2^- + H_2O \Leftrightarrow Al(OH)_4^-$

(7) $trans\text{-}AlO(OH)_2^- + H_2O \Leftrightarrow Al(OH)_4^-$

(8) $Al(OH)_3 + H_2O \Leftrightarrow Al(OH)_3(H_2O)$

(9) $Al(OH)_4^- + H_2O \Leftrightarrow Al(OH)_4(H_2O)^-$

(10) $Al(OH)_4(H_2O)^- + H_2O \Leftrightarrow Al(OH)_4(H_2O)_2^-$

(11) $Al(OH)_5^{2-} + H_2O \Leftrightarrow Al(OH)_5(H_2O)^{2-}$

(12) $Al(OH)_4^- + 4H_2O \Leftrightarrow Al(OH)_4(H_2O)_4^-$

TABLE 4: Reaction Energies (kJ mol^{-1}), Including Zero-Point Energy Differences, for the Processes Given in Scheme 1 at the MP2(fc)/6-31G, B3LYP/6-31G**, and B3LYP/6-311++G** Levels of Calculation in the Gas Phase and also for the Hybrid Density Functional Method with the Highest Basis Set Employed as a Single-Point Calculation Embedded in the SCI-PCM Model with a Dielectric Constant of 80.4**

	MP2(fc)/6-31G**	B3LYP/6-31G**	B3LYP/6-311++G**	
reaction	gas phase	gas phase	gas phase	dilute soln
(1)	−508.08	−504.16	−360.12	−251.68
(2)	+156.39	+159.73	+267.10	+10.60
(3)	+594.49	+595.49	+656.95	+107.32
(4)	−272.10	−276.30	−242.73	−221.61
(5)	−251.47	−255.75	−222.19	−214.19
(6)	−297.44	−292.33	−261.38	−220.97
(7)	−318.07	−312.88	−281.92	−228.39
(8)	−105.25	−101.13	'−69.63	−56.86
(9)	−79.08	−79.36	−57.02	−27.35
(10)	−67.75	−67.09	−55.05	−20.07
(11)	−142.96	−142.23	−114.67	−38.40
(12)	−256.24	−265.38	−181.37	−70.00

TABLE 5: Reaction Energies (kJ mol^{-1}), Including Zero-Point Energy Differences, for the Processes Given in Scheme 1 at the B3LYP/6-311++G//B3LYP/6-31G** Level of Calculation, Depending on the Number of Hydration Shells in the Electrostatic Embedding Model[a]**

reaction	0 shells	1 shell	2 shells	3 shells
(1)	−348.120	−467.626	−488.173	−495.228
(2)	−132.269	−47.122	+8.640	+41.464
(3)	−110.697	+173.886	+298.993	+367.287
(4)	−252.232	−269.491	−273.147	−274.488
(5)	−207.526	−241.778	−249.174	−251.935
(6)	−287.728	−291.050	−291.738	−291.990
(7)	−332.435	−318.764	−315.712	−314.544
(9)	−42.725	−67.854	−73.828	−76.120
(10)	−33.615	−55.384	−61.231	−63.580
(11)	+22.198	−89.887	−116.87	−127.313
(12)	−185.266	−232.382	−244.531	−249.302

[a] Note that reaction 8 is omitted as there is no electrostatic effect due to all species being neutral.

polarization basis set, the energy for addition of an extra hydroxyl to the tetrahedral aluminate is erroneously slightly exothermic. For a truly accurate estimate of the energy difference it would be necessary to include the first solvent shell explicitly in addition to the polarizable continuum model. However, this is not practical for all species considered in this study.

3.1.2. Stability of Monomers in Concentrated Liquors. The electrostatic model, in which the presence of countercations is approximately accounted for, offers the possibility of assessing the likely effect of solution concentration based upon how many hydration shells are present (see Table 5). The effect of the electrostatic model on the formation of the tetrahedral aluminate anion from $Al(OH)_3$ is to add a positive term to the reaction energy, again due to the small size of the hydroxide species. However, the process is still strongly exothermic overall for all degrees of solvation. Conversely, the formation of multiply-charged aluminate anions is very sensitive to the number of hydration shells. The five-coordinate $Al(OH)_5^{2-}$ species is predicted to be stable in the presence of excess hydroxide at high concentrations, where only a single layer of water separates the sodium cations from the aluminate anion. In typical Bayer liquors, the amount of water available is probably sufficient for between 1 and 2 hydration shells, thus implying that some formation of dianions may be possible, though they are unlikely to be the dominant species.

Under extreme conditions of dehydration and basicity it is predicted that even the formation of $Al(OH)_6^{3-}$ might be possible, provided ion pairing occurs. Although the results for the zero hydration case must be considered as very crude indeed, preliminary results involving the explicit inclusion of sodium confirm that this result is qualitatively, though not quantitatively, correct. Given the level of water actually present experimentally, it is very unlikely that this anion will have a significant concentration, as it becomes unstable with any amount of water separating the ion pairs.

The effect of the degree of hydration on the other reactions considered for interconversion of monomeric aluminum species is relatively small and in only one other case does it cause a transition from endothermic to exothermic behavior or vice versa. This one case is the binding of a water molecule to the dianion $Al(OH)_5^{2-}$. Because of the approximation of a fixed spherical distribution of counterions, the addition of a water of hydration leads to a significant loss of electrostatic stabilization, thus making the solvation unfavorable. In a more accurate model this effect would be unlikely to occur.

It appears from the various equilibria that singly charged anions will be the dominant monomeric aluminate species both in dilute and concentrated solutions, except where ion pairing starts to occur. However, there are a range of possible anions in this category with varying coordination numbers from two (AlO_2^-) to six ($Al(OH)_4(H_2O)_2^-$). The energies for the reaction of both the two- and three-coordinate anions with water are exothermic in the gas phase, leading to formation of the tetrahedral aluminate anion. One apparent anomaly is that, in dilute solution, it appears that both of the $AlO(OH)_2^-$ species are unstable with respect to disproportionation, with both AlO_2^- and $Al(OH)_4^-$ being more stable. This situation arises because of the very high hydration energy of the small AlO_2^- anion. In the case of such anions, the solvation energy will be greatly decreased by explicit inclusion of the first hydration shell, and therefore the value obtained from the polarizable continuum model must be regarded as significantly in error in this situation as the AlO_2^- anion is almost certainly unstable in dilute solution.

The binding of one or two further water molecules to the tetrahedral anion is also exothermic. In these cases, the water molecules were initially positioned with oxygen coordinated to aluminum prior to optimization. Following energy minimiza-

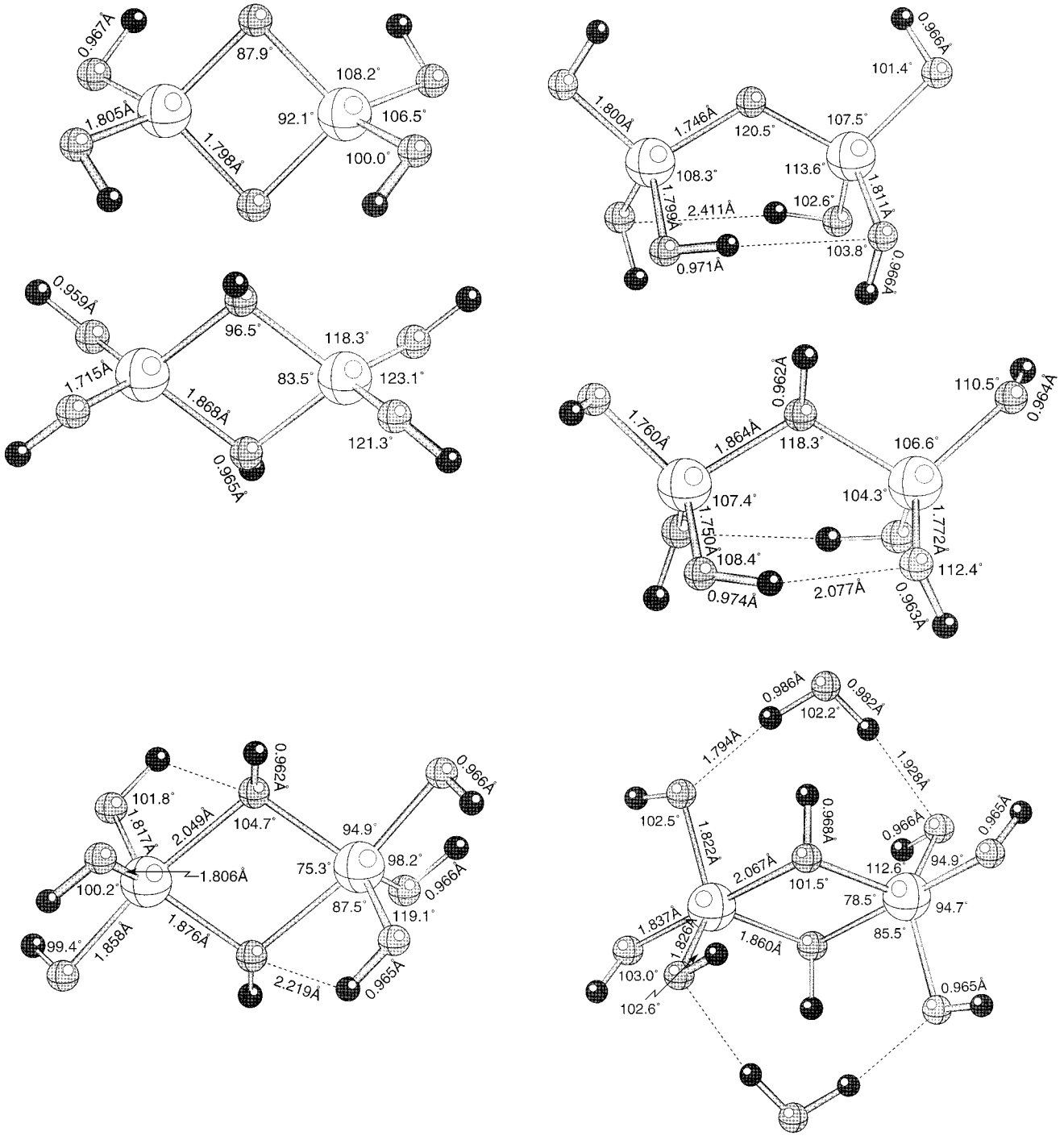

Figure 2. Optimized structures at the B3LYP/6-31G** level of calculation for the dimeric aluminate species, including selected symmetry unique bond lengths and angles. Aluminum atoms are colored in light grey, oxygen in mid-grey, and hydrogens are dark grey.

tion, the water leaves the coordination sphere of aluminum to become water of hydration by forming two hydrogen bonds bridging between hydroxyl oxygen atoms, as shown in Figure 1. This arrangement leads to the strongest binding of water and results in a narrowing of the water bond angle to around 98° in order to maximize both hydrogen bonds. If four water molecules are introduced to solvate the anion, a different configuration is adopted in which water acts as a donor and acceptor in a six-ring geometry. However, the hydrogen bond from the OH of aluminate to water is rather weak.

It appears that under basic conditions, tetrahedral coordination is favored and only binding of further hydroxyls, rather than water, can increase the coordination number. This is the opposite of the situation found under acidic conditions where octahedral coordination dominates. Solvation of the anions appears to occur preferentially by hydrogen bonding to the oxygen of aluminate as the hydrogen atoms fail to form strong interactions with water.

All of the above confirms that the most stable species in dilute basic solution should be the tetrahedral aluminate anion, as expected. Even in concentrated basic conditions other monomers tend to be unfavorable, although there is some possibility of forming $Al(OH)_5^{2-}$ in very anhydrous liquors. A more definite conclusion about the stability of this species relative to the monoanion would require explicit inclusion of the first solvation shell of water and countercations. Even so, there

SCHEME 2: Reaction Scheme for Possible Dimerization Reactions of Aluminum Monomers and for the Equilibria between Dimers

(1) $2Al(OH)_4^- \Leftrightarrow Al_2(OH)_8^{2-}$

(2) $2Al(OH)_4(H_2O)^- \Leftrightarrow Al_2(OH)_8(H_2O)_2^{2-}$

(3) $2Al(OH)_4^- \Leftrightarrow Al_2(OH)_7^- + OH^-$

(4) $Al(OH)_4^- + Al(OH)_3 \Leftrightarrow Al_2(OH)_7^-$

(5) $2Al(OH)_4^- \Leftrightarrow Al_2O(OH)_6^{2-} + H_2O$

(6) $2\ cis\text{-}AlO(OH)_2^- \Leftrightarrow Al_2O_2(OH)_4^{2-}$

(7) $2\ trans\text{-}AlO(OH)_2^- \Leftrightarrow Al_2O_2(OH)_4^{2-}$

(8) $Al_2O(OH)_6^{2-} + H_2O \Leftrightarrow Al_2(OH)_7^- + OH^-$

(9) $Al_2(OH)_7^- + OH^- \Leftrightarrow Al_2(OH)_8^{2-}$

(10) $Al_2(OH)_8^{2-} \Leftrightarrow Al_2O_2(OH)_4^{2-} + 2H_2O$

remains the problem of a vast region of configuration space to be explored and the effects of the dynamics of the system.

3.2. Dimer Species. While the consideration of the stability of monomeric species at high solution concentrations is important, it is likely that under such conditions higher-order aluminum-containing oligomers will begin to form. Ultimately, the precipitation of aluminum hydroxide will occur from supersaturated solutions, as gibbsite, bayerite, or nordstrandite, depending on reaction conditions, for example temperature. However, the formation of the precipitate is known to be slow and is thus likely to be integration controlled, rather than bulk diffusion controlled.[34] Thus, it is crucial to characterize the nature of the growth units that incorporate into a growing crystal, as well as the nature of any intermediate species, so that the rate-limiting steps in crystallization can be determined. In this section, we will concentrate on the formation of dimeric species, and studies of higher oligomers will be confined to future work.

There has been much speculation as to the most abundant dimer that forms in alkaline solution.[2,5,35] A strong possibility is the $Al_2(OH)_7^-$ anion, in which a single hydroxyl group bridges between the two aluminum atoms, as this has been demonstrated to be present in a number of crystal structures.[7]

Several dimer species may be conceived of, on the basis of cross-linking of aluminum via either one or two oxide or hydroxide anions. Any more than two common species between aluminum atoms can be ruled out as face-sharing octahedra are rarely found in the absence of metal−metal bonding and this coordination geometry plays no part in the structural chemistry of aluminum hydroxides. The optimized structures of the dimers at the B3LYP/6-31G** level considered in this work are shown in Figure 2.

When two species bridge between the aluminum atoms, this can be seen to introduce strain into the bond angles. For instance, in $Al_2(OH)_7^-$ the Al−O(H)−Al angle is 118.3°, whereas when two hydroxyls bridge this is reduced to 96.5°. The double oxo-bridge is even more strained being almost square with angles of 87.9° and 92.1° at oxygen and aluminum, respectively. In $Al_2(OH)_8^{2-}$, which also contains a double-hydroxo bridge, the Al−O(H) distances are no longer symmetrical, with values of 1.876 and 2.049 Å. This occurs as a result of intramolecular hydrogen bonding between a terminal hydroxyl and a bridging one, despite the fact that the bond is quite long and weak. Coordination of two water molecules to $Al_2(OH)_8^{2-}$ can readily be achieved. However, as in the case of the monomers, the water fails to coordinate to aluminum to make it octahedral, but instead bridges across the cluster to form two hydrogen bonds each.

Intramolecular hydrogen bonding is also found for $Al_2(OH)_7^-$ between hydroxyls coordinated to different aluminum atoms. This is exactly what is observed for dimer models for zeolites when hydroxyl termination is used.[36] Arguably, these interactions occur only in the gas phase for this cluster and would be lost in favor of intermolecular hydrogen bonds when solvated.

TABLE 6: Reaction Energies (kJ mol^{-1}), Including Zero-Point Energy Differences, for the Possible Dimer Formation Processes Given in Scheme 2 at the MP2(fc)/6-31G, B3LYP/6-31G**, and B3LYP/6-311++G** Levels of Calculation in the Gas Phase and also for the Hybrid Density Functional Method with the Highest Level of Basis Set Employed as a Single-Point Calculation Embedded in the SCI-PCM Model with a Dielectric Constant of 80.4**

	MP2(fc)/6-31G**	B3LYP/6-31G**	B3LYP/6-311++G**	
reaction	gas phase	gas phase	gas phase	dilute soln
(1)	+206.649	+231.775	+254.84	+44.84
(2)	+154.593	+182.575	+212.53	+23.61
(3)	+250.573	+260.721	+165.49	+105.70
(4)	−257.507	−243.395	−194.63	−145.98
(5)	+265.342	+278.438	+297.29	+42.59
(6)	−158.190	−130.590	−70.02	−310.57
(7)	−199.447	−171.685	−111.09	−325.40
(8)	−14.768	−17.717	−131.80	+63.11
(9)	−43.925	−28.946	+89.36	−60.86
(10)	+230.034	+222.294	+197.90	+86.54

TABLE 7: Reaction Energies (kJ mol^{-1}), Including Zero-Point Energy Differences, for the Possible Dimer Formation Processes Given in Scheme 2 at the B3LYP/6-311++G//B3LYP/6-31G** Level of Calculation, Depending on the Number of Hydration Shells in the Electrostatic Embedding Model**

reaction	0 shells	1 shell	2 shells	3 shells
(1)	+10.697	+63.072	+101.364	+126.296
(2)	−104.332	−7.024	+42.147	+71.246
(3)	+173.672	+246.924	+255.908	+258.412
(4)	−174.403	−220.657	−232.220	−236.771
(5)	+35.334	+100.934	+143.508	+170.222
(6)	−434.404	−329.445	−276.295	−245.280
(7)	−523.817	−384.872	−324.242	−290.387
(8)	+138.338	+145.969	+112.400	+88.190
(9)	−162.975	−183.852	−154.544	−132.116
(10)	+130.356	+189.584	+205.818	+212.405

3.2.1. Stability of Dimers in the Gas Phase and Dilute Solution. As in the case of the monomers, a number of reactions, shown in Scheme 2, which lead to the creation of dimers or interconversion between different dimers have been postulated. Once again, the energies for these processes have been calculated in the gas phase at the MP2(fc)/6-31G**, B3LYP/6-31G**, and B3LYP/6-311++G**//B3LYP/6-31G** levels as tabulated in Table 6. In addition, corrections appropriate for a dilute solution have also been evaluated using a self-consistent polarizable continuum approach for the latter density functional case.

Nearly all anion−anion condensations are unfavorable in the gas phase due to the obvious electrostatic repulsion, with the exception of both three-coordinate aluminum anions, where the underlying instability of the species due to the low coordination number is sufficient to overcome the electrostatic penalty. However, this does not represent a favorable overall route for dimerization due to the highly endothermic heat of formation for the $AlO(OH)_2^-$ ions.

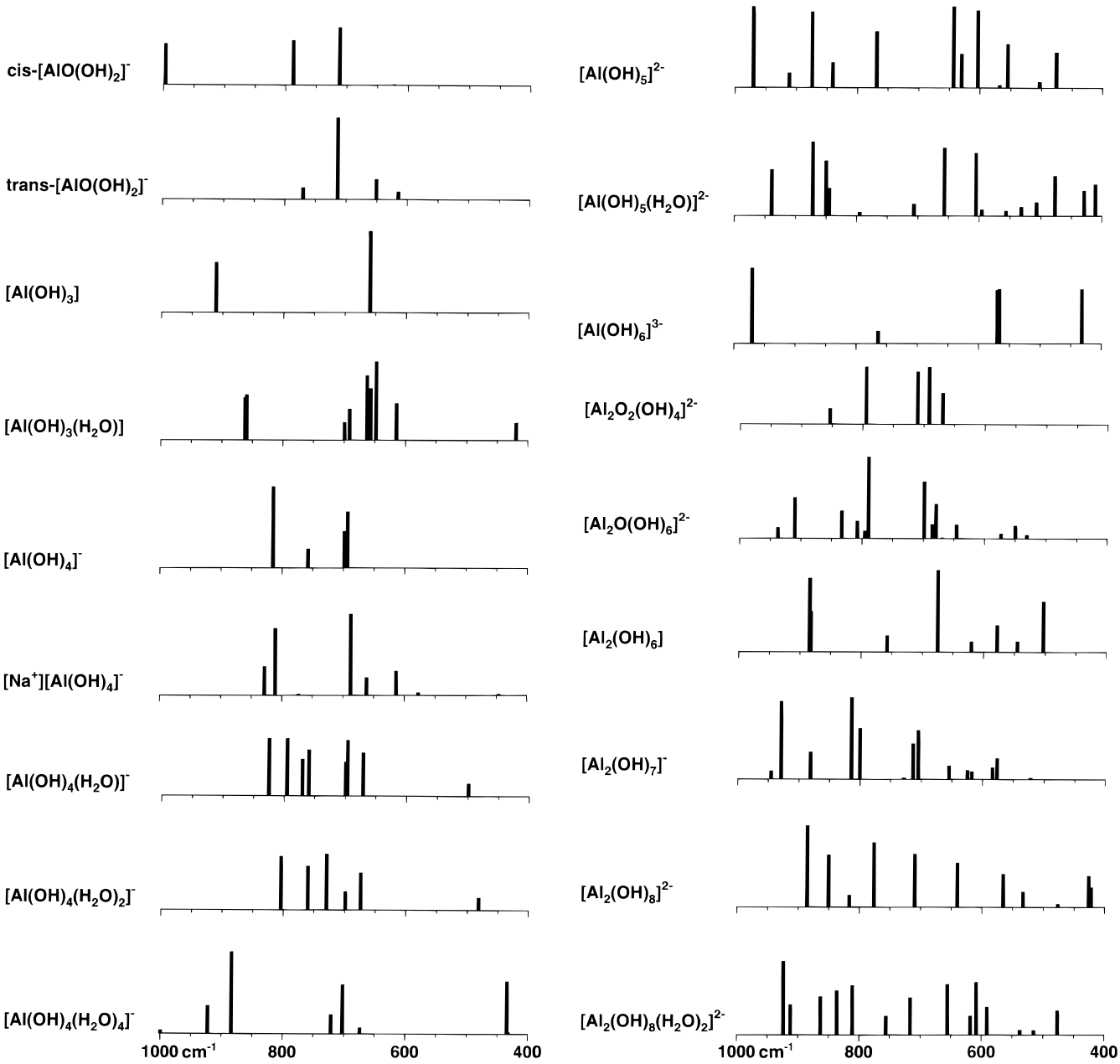

Figure 3. Calculated infrared spectra for monomeric and dimeric aluminate species at the B3LYP/6-31G** level of calculation in the frequency range 400−1000 cm^{-1}. Note that the frequencies have been scaled by 0.9614.

While the calculated reaction energies involving monomeric species were generally very similar at both the MP2(fc) and B3LYP levels, there is a much greater discrepancy for the dimerization energetics. Even allowing for the fact that the system sizes involved are larger and that the error is an extensive property, the differences are far larger pro rata. Although zero-point energies are systematically larger at the MP2 level (in the absence of scaling), this is not the dominant contribution to the energy differences between the calculation levels.

The calculated stabilities of the dimers in dilute aqueous solution are significantly different from the gas phase. Now, two dimerization processes starting from tetrahedral aluminate and forming either a double-hydroxo-bridged dimer, $Al_2(OH)_8^{2-}$, or an oxo-bridged dimer, $Al_2O(OH)_6^{2-}$, are only marginally endothermic. In fact, the inclusion of explicit water of hydration in the former species is sufficient to make the reaction exothermic overall. Hence, within the limits of the accuracy of the calculation and the representation of the environment it is hard to be certain whether the process is endo- or exothermic, although it is clear that *dimerization is energetically feasible.* An earlier study[35] suggested that the double hydroxy-bridged species would dehydrate to form the oxo-bridged dimer, though as these results were obtained for the gas phase at the STO-3G//MNDO level, the present results are likely to be more reliable. Interestingly, the dimer species with a single hydroxo bridge between the aluminum atoms, $Al_2(OH)_7^-$, which has been reported to exist in the solid state,[7] appears to be unstable with respect to the above two dimers.

3.2.2. Stability of Dimers in Concentrated Liquors. From the perspective of the electrostatic model, on the basis of the results given in Table 7, a similar qualitative picture emerges as for the dilute solution environment. The same two dimer species appear to be the most stable with the mono-hydroxo-bridged dimer again being unstable with respect to disproportionation. The main quantitative difference is that the dimerization rapidly becomes more endothermic as the number of

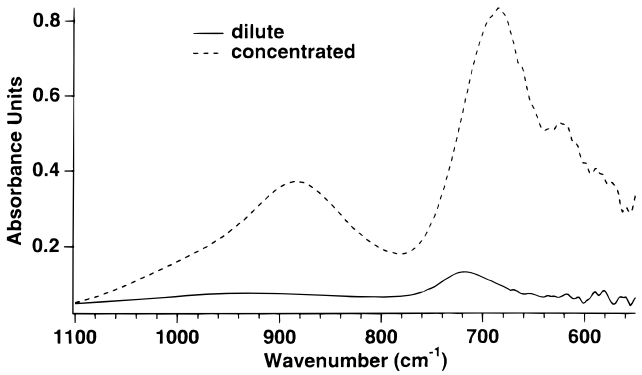

Figure 4. Experimental infrared spectra of dilute (0.59 M $NaAl(OH)_4$ with 1.30 M excess NaOH) and concentrated (6.86 M $NaAl(OH)_4$ with 2.57 M excess NaOH) aluminate solutions. Spectra were collected according to the methods described in ref 37. A constraint is that water absorption prevents the acquisition of data below 550 cm^{-1}.

hydration shells increases. This is perhaps a more reasonable picture than the one obtained from the polarizable continuum embedding, as it implies that formation of oligomers will only start to take place as the aluminate ion concentration increases under basic conditions. As before, more accurate representation of the hydration shells and countercations is needed before a quantitative prediction can be made of the concentration required before dimerization becomes energetically feasible.

3.3. Infrared Spectra of Aluminate Species. On the basis of a consideration of the reaction energetics, a picture of the likely aluminum species under basic conditions has been formulated, both for dilute and concentrated solutions. The critical question now is whether these predictions are consistent with the experimental evidence. The most widely used spectroscopic techniques for the experimental study of aluminate solution structure are infrared and Raman spectroscopy.[37] Although the latter is generally the method of preference from an experimental point of view, quantum mechanical calculation of infrared intensities is more practical. Hence, comparison will be made between the calculated infrared spectra (Figure 3) and the experimental observations (Figure 4). All spectra have been calculated at both the MP2/6-31G** and B3LYP/6-31G** levels, although only the latter are illustrated in the figure as both are very similar to within a scaling factor. To correct for the systematic errors in the frequencies associated with the computational method used, the density functional values have been scaled by 0.9614.[38]

The experimental infrared spectrum for the dilute sodium aluminate solution in Figure 4 shows a peak at 720 cm^{-1} and a broad feature at 900 cm^{-1}. Between these peaks, in the region of 800 cm^{-1} there are no other infrared active modes. The calculated spectrum for the most probable aluminate anion, $Al(OH)_4^-$, is found to have its most intense vibration at close to 800 cm^{-1} which is inconsistent with the experimental data. However, this is for the gas-phase molecule, so spectra of aluminate ions with varying numbers of water molecules solvating them should also be taken into consideration. When one or two water molecules coordinate by hydrogen bonding between two oxygen atoms of the aluminate ion, the vibrational spectra become increasingly complex. However, there is no overall shift of the modes leading to an explanation of the observed spectrum.

In contrast, when the aluminate anion becomes completely solvated by four water molecules, which is the most probable coordination environment in a dilute solution, this results in a spectrum which consists of two broad peaks close to 950 cm^{-1} and two in the region 700−720 cm^{-1}. On this basis, it is concluded that $Al(OH)_4(H_2O)_4^-$ with its excellent agreement between predicted and observed infrared spectra, is indeed the species most likely to be present in dilute solution.

As the concentration of the sodium aluminate solution increases, a number of changes are observed in the experimental infrared spectrum. The peaks observed under dilute conditions appear to be shifted downward to 880 and 680 cm^{-1}. In fact, the apparent shift in the 950 cm^{-1} peak is due to the emergence of a new peak at 860 cm^{-1}. An additional new peak appears at 630 cm^{-1}. Examination of the calculated dimer spectra shows that none of the species represent an exact match for the observed peaks. However, given the complexity of the liquors, it is unlikely that a single polyanion alone is entirely responsible. Perhaps the most likely of the dimers, based on comparison of the vibrational modes, is $Al_2(OH)_8(H_2O)_2^{2-}$ as this shows an intense peak close to 950 cm^{-1} and several peaks clustered in the region of 630 cm^{-1}. Given that this is also the energetically favored dimer, this may be the species which gives rise to the two new bands which are observed in spectra, though more extensive calculations will be needed to confirm this.

Molecular dynamics simulations have demonstrated the presence of contact pairing between Na^+ and $Al(OH)_4^-$ ions in concentrated aluminate solutions.[39] Hence, the complex $Na^+Al(OH)_4^-$ has also been included in the calculated spectra. The predicted infrared spectrum for this contact ion pair has several features in common with the experimental observations. The main peaks are similar to those of the hydrated aluminate anion, but shifted to lower frequency. Although the highest peak is a little low to be the one at 860 cm^{-1}, the most intense peak falls at 680 cm^{-1} and there is also a peak close to the observed position at 630 cm^{-1}. Partial hydration will alter this picture slightly and may explain the fact that the highest mode is marginally too low. Due to the need to consider the hydration shells of both Na^+ and $Al(OH)_4^-$, determination of spectrum of the hydrated contact pair is computationally very demanding and is currently being investigated.

Although it is hard to make conclusive interpretations of the experimental infrared spectra in the context of the predicted ones, since the degree of solvation perturbs the vibrational frequencies, it does appear that the energetically favored species are the best candidates for tentative assignments to the observed data. While the difficulty increases for the concentrated aluminate solutions, the observed infrared spectrum may be due to a combination of a dimer species, most probably $Al_2(OH)_8(H_2O)_2^{2-}$ and the contact ion pair between sodium and $Al(OH)_4^-$.

4. Conclusions

The structure and stability of a wide range of possible monomeric and dimeric aluminate species have been studied at the MP2(fc)/6-31G** and B3LYP/6-311++G**//B3LYP/6-31G** levels of calculation. Generally, we find good agreement between geometries, energies, and scaled vibrational frequencies calculated using either methodology. This will make it practical to extend the present work to higher order oligomers in the future.

The greatest challenge facing the study of Bayer liquors is to adequately model the influence of the surrounding environment, as gas-phase calculations alone are clearly meaningless when considering the condensation of anions. In the present work, two simple approaches to achieving this have been considered; either the ions are embedded in a dielectric continuum to mimic the dilute solution limit or the anions are surrounded by a charge-compensating set of point charges to model the high concentration limit. In both cases, it is desirable

to at least include the first shell of coordinated ions and solvent explicitly, although this was not practical for all cases in the present study. In the case of the $Al(OH)_4^-$ anion, inclusion of the first complete hydration shell led to agreement between the calculated and experimental infrared spectra for the dilute aluminate solution.

Under dilute conditions, it appears that $Al(OH)_4(H_2O)_4^-$ is the energetically preferred species in accord with expectation, although in the presence of excess hydroxide and higher concentrations, it is possible that some $Al(OH)_5^{2-}$ may be formed. Any water of solvation for the monomers is found to hydrogen bond to the oxygen atoms of the aluminate ion and not to coordinate directly to aluminum.

As the solutions become more concentrated and dimerization occurs, the most stable species would appear to be the doubly hydroxo-bridged species $(OH)_3Al(OH)_2Al(OH)_3^{2-}$ with at least two waters of hydration. This is found to be more stable than the complex with only one hydroxyl group separating the aluminum atoms, $[(OH)_3AlOAl(OH)_3]^{2-}$, which is more often proposed to be the predominant dimer on the basis of known crystal structures.[5] Given that the final aluminum hydroxide structure contains two bridging hydroxyl groups, as do proposed higher oligomers, it is quite reasonable to expect the above calculated prediction to be correct. Comparison of the calculated and measured infrared spectra for more concentrated sodium aluminate solutions appears to support the above species being one of the components present, although there are almost certainly others as well, which probably include the $Na^+Al(OH)_4^-$ ion pair.

Further work is now needed to examine the effects of including more of the environment (e.g., water and sodium ions) explicitly within the quantum mechanics, especially their role in stabilizing ion pairs, dimers, and higher oligomers. Also, the question of the kinetics of the dimerization remains an important issue to be addressed in order to understand the rate of crystallization.

Acknowledgment. J.D.G. thanks the Royal Society for a University Research Fellowship and the EPSRC for provision of computing facilities. The financial support of the Australian Federal Government through its Cooperative Research Centres Program is also gratefully acknowledged.

References and Notes

(1) Eremin, N. I.; Volokhov, Y. A.; Mironov, V. E. *Russ. Chem. Rev.* **1974**, *43*, 92.
(2) Zambo, J. *Light Metals* **1986**, 199.
(3) Sipos, P.; May, P. M.; Hefter, G. T.; Kron, I. *J. Chem. Soc., Chem. Commun.* **1994**, 2355.
(4) Lippincott, E. R.; Psellos, J. E.; Tobin, M. C. *J. Chem. Phys.* **1952**, *20*, 536.
(5) Moolenaar, R. J.; Evans, J. C.; McKeever, L. D. *J. Phys. Chem.* **1970**, *74*, 3629.
(6) Wajand, J.; Szabo, Z. G.; Ruff, I.; Burger, K. *Magy. Kem. Foly.* **1980**, *86*, 339.
(7) Johansson, G. *Acta Chem Scand.* **1966**, *20*, 505.
(8) Saalfeld, H.; Wedde, M. *Z. Kristallogr.* **1974**, *139*, 129.
(9) Rossiter, D. S.; Fawell, P. D.; Ilievski, D.; Parkinson, G. M. *J. Crystal Growth* **1998**, *191*, 525.
(10) Akitt, J. W.; Gessner, W. *J. Chem. Soc., Dalton Trans.* **1984**, 147.
(11) Bradley, S. M.; Hanna, J. V. *J. Chem. Soc., Chem. Commun.* **1993**, 1249.
(12) Bradley, S. M.; Hanna, J. V. *J. Am. Chem. Soc.* **1994**, *116*, 7771.
(13) Sipos, P.; Bodi, I.; May, P.; Hefter, G. In *Progress in Coordination and Organometallic Chemistry*, Ondrejovic, G., Sirota, A., Eds.; Slovak Technical University Press: Bratislava, **1997**; p 303.
(14) Buvaribarcza, A.; Rozsahegyi, M.; Barcza, L. *J. Mater. Chem.* **1998**, *8*, 451.
(15) Gerson, A. R.; Ralston, J.; Smart, R. St. C. *Colloids Surf., A* **1996**, *110*, 105.
(16) Hess, A. C.; McMillan, P. F.; O'Keefe, M. *J. Phys. Chem.* **1988**, *92*, 1785.
(17) Kubicki, J. D.; Apitz, S. E.; Blake, G. A. *Phys. Chem. Miner.* **1995**, *22*, 481.
(18) Ruiz, J. M.; McAdon, M. H.; Garcés, J. M. *J. Phys. Chem.* **1997**, *101*, 1733.
(19) Pelmenschikov, A. G.; Morosi, G.; Gamba, A. *J. Phys. Chem.*, **1991**, *95*, 10037.
(20) Matsuo, T.; Kobayashi, K.; Tago, K. *J. Phys. Chem.* **1996**, *100*, 6531.
(21) Becke, A. D. *J. Chem. Phys.* **1993**, *98*, 5648.
(22) Lee, C.; Yang, W.; Parr, R. G. *Phys. Rev.* **1988**, *B37*, 785.
(23) Fitzgerald, G.; Anzelm, J. *J. Phys. Chem.* **1991**, *95*, 10531.
(24) Murray, C. W.; Laming, G. J.; Handy, N. C.; Amos, R. D. *Chem. Phys. Lett.* **1992**, *199*, 551.
(25) Ditchfield, R.; Hehre, W. J.; Pople, J. A. *J. Chem. Phys.* **1971**, *54*, 724.
(26) Frisch, M. J.; Trucks, G. W.; Schlegel, H. B.; Gill, P. M. W.; Johnson, B. G.; Robb, M. A.; Cheeseman, J. R.; Keith, T.; Petersson, G. A.; Montgomery, J. A.; Raghavachari, K.; Al-Laham, M. A.; Zakrzewski, V. G.; Ortiz, J. V.; Foresman, J. B.; Cioslowski, J.; Stefanov, B. B.; Nanayakkara, A.; Challcombe, M.; Peng, C. Y.; Ayala, P. Y.; Chen, W.; Wong, M. W.; Andres, J. L.; Replogle, E. S.; Gomperts, R.; Martin, R. L.; Fox, D. J.; Binkley, J. S.; Defrees, D. J.; Baker, J.; Stewart, J. P.; Head-Gordon, M.; Gonzalez, C.; Pople, J. A. Gaussian94, Revision D.3; Gaussian Inc.: Pittsburgh, PA, 1995.
(27) Craw, J. S.; Greatbanks, S. P.; Hillier, I. H.; Harrison, M. J.; Burton, N. A. *J. Chem. Phys.* **1997**, *106*, 6612.
(28) Li, J.; Fisher, C. L.; Chen, J. L.; Bashford, D.; Noodleman, L. *Inorg. Chem.* **1996**, *35*, 4694.
(29) (a) Miertus, S.; Scrocco, E.; Tomasi, J. *Chem. Phys.* **1981**, *55*, 117. (b) Keith, T. A.; Frisch, M. J. *ACS Symp. Series*, **1994**, *569*, 22.
(30) Parchment, O. G.; Vincent, M. A.; Hillier, I. H. *J. Phys. Chem.* **1996**, *100*, 9689.
(31) Singh, U. C.; Kollman, P. A. *J. Comp. Chem.* **1984**, *5*, 129.
(32) Saalfeld, H.; Wedde, M. *Z. Kristallogr.* **1974**, *139*, 129.
(33) Tuñón, I.; Rinaldi, D.; Ruiz-López, M. F.; Rivail, J. L. *J. Phys. Chem.* **1995**, *99*, 3798.
(34) Mullin, J. W. In *Crystallization*, 3rd ed.; Butterworth-Heinemann: Oxford, 1993.
(35) Liu, H.; Huang, S.; Chen, N. *Trans. Non-Ferrous Metals Soc. China* **1992**, *2*, 43.
(36) Sauer, J.; Ugliengo, P.; Garrone, E.; Saunders, V. R. *Chem. Rev.* **1994**, *94*, 2095.
(37) Watling, H. *Appl. Spectrosc.* **1998**, *52*, 250.
(38) Scott, A. P.; Radom, L. *J. Phys. Chem.* **1996**, *100*, 16502.
(39) Watling, H. R.; Fleming, S. D.; van Bronswijk, W.; Rohl, A. L. *J. Chem. Soc. Dalton Trans.*, in press.